

Generalization Dynamics of Linear Diffusion Models

Claudia Merger and Sebastian Goldt*

International School of Advanced Studies (SISSA), Trieste, Italy

10th June 2025

Abstract

Diffusion models trained on finite datasets with N samples from a target distribution exhibit a transition from memorisation, where the model reproduces training examples, to generalisation, where it produces novel samples that reflect the underlying data distribution. Understanding this transition is key to characterising the sample efficiency and reliability of generative models, but our theoretical understanding of this transition is incomplete. Here, we analytically study the memorisation-to-generalisation transition in a simple model using linear denoisers, which allow explicit computation of test errors, sampling distributions, and Kullback-Leibler divergences between samples and target distribution. Using these measures, we predict that this transition occurs roughly when $N \asymp d$, the dimension of the inputs. When N is smaller than the dimension of the inputs d , so that only a fraction of relevant directions of variation are present in the training data, we demonstrate how both regularization and early stopping help to prevent overfitting. For $N > d$, we find that the sampling distributions of linear diffusion models approach their optimum (measured by the Kullback-Leibler divergence) linearly with d/N , independent of the specifics of the data distribution. Our work clarifies how sample complexity governs generalisation in a simple model of diffusion-based generative models and provides insight into the training dynamics of linear denoisers.

1 Introduction

Diffusion models [1, 2, 3] have become the state-of-the-art paradigm in generative AI, where they are trained to sample from an unknown distribution ρ based on a finite set of training data, sampled from ρ . Diffusion models sample by implementing a function that maps a random seed into a new sample. While the behavior of diffusion models that have learned this mapping accurately has been studied recently [4, 5, 6, 7, 8, 9], much less is known about their behavior when trained on finite datasets.

In this context, Kadkhodaie et al. [10] recently made a remarkable observation: diffusion models trained on finite datasets with N samples from a target distribution exhibit a transition from memorisation, where the model reproduces training examples, to generalisation, where it produces novel samples that reflect the underlying data distribution. We illustrate this phenomenon in fig. 1a), where we show samples generated by diffusion models optimized on training sets of increasing size N . For each sampled image, we show the most similar image from the training set in fig. 1b). We find that for the CelebA dataset [11], for training set sizes up to $N = 3200$, new samples can be identical to the training examples, meaning that the latter are essentially memorized, before genuinely new samples emerge at $N \geq 6400$. Beyond comparing the samples manually, we quantify memorization by measuring the similarity between elements of the training set and the generated samples, which decreases with N , see fig. 1 c).

But does the absence of memorization mean the model has found a general solution? A crucial observation by Kadkhodaie et al. [10] was that two models trained on large, but independent sets of

*{cmerger, sgoldt}@sisssa.it

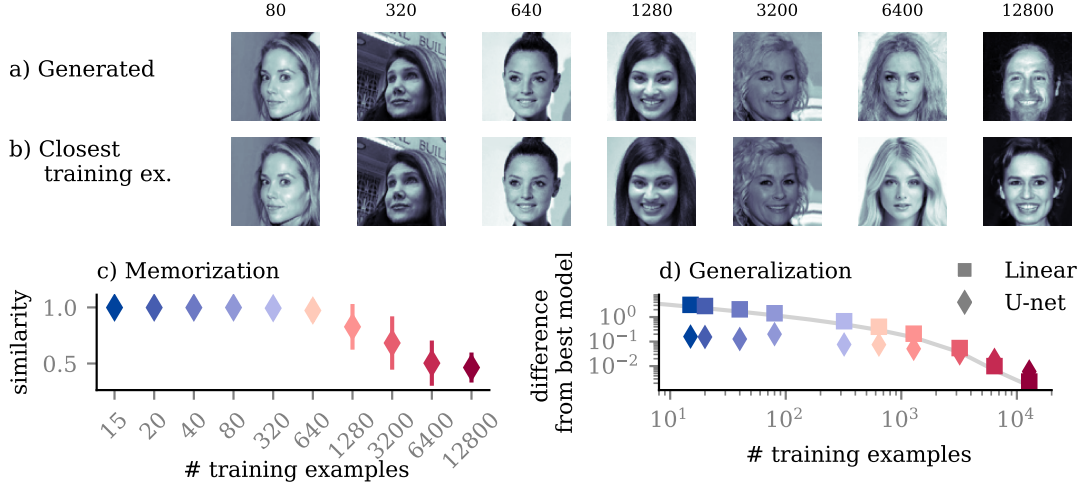


Figure 1: a) Samples generated from diffusion models with a U-net architecture at different training set sizes N . b) Most similar elements of the corresponding training set. d) Average similarity (averaged over 10^2 samples, error bars report one standard deviation) between samples generated from diffusion models with U-net architectures and training set, measured with emphasis on details in the images (for details, see appendix A). All training data sets of all models are disjoint. a) Squared differences between the mappings of diffusion models trained from a reference model trained on $N_{\max} = 6 \cdot 10^4$ training examples, averaged over 10 test examples in the linear and 10^2 test examples in the non-linear case. Error bars reporting standard deviations are smaller than the symbol sizes.

data can produce the same sample given the same random seed, meaning that they must essentially implement the same mapping. We measure the similarity between the mappings by comparing diffusion models of different architectures (Linear and U-net) trained on subsets of increasing size of CelebA to a reference model trained on $N = 6 \cdot 10^4$ samples. In fig. 1d), we show that the difference from the reference model on test examples from a the reference model trained on decays with N . This indicates that the models implement a solution that is increasingly independent of the details of the training set, but rather general, as it depends on characteristic statistics of ρ .

These observations raise two intriguing questions: First, how many samples are required such that the model no longer memorizes the data? Second, how many samples are necessary for the mappings of different diffusion models to align?

In this work, we present a theory of the memorization-generalization transition for linear diffusion models. Linear neural networks have helped elucidate overfitting in supervised learning in the past [12, 13] by providing a fully tractable case in which key mechanisms can be understood. Here, assuming that the denoiser is a linear neural network allows to connect data structure, learning dynamics, regularization, the training outcomes at finite N in an analytical theory. Specifically, our main contributions are the following:

- We derive the test and training loss as well as the Kullback-Leibler divergence between the sampling and target distribution for a diffusion model with linear denoiser.
- We show that overfitting is most severe when $N < d$, where relevant directions of variation in ρ are not present in the training set, and we show how both early stopping and regularization are effective measures to prevent overfitting
- We show that in the $N > d$ regime, the Kullback-Leibler divergence between the sampling distribution and ρ decays linearly in $\frac{d}{N}$, independent of the details of the target distribution.
- We finally observe that the mappings implemented by non-linear denoisers are similar to the mappings learnt by linear denoisers for a wide range of diffusion times and eigenmodes of the input covariance, and that the differences grow with the number of samples N .

Further related work

A growing body of work studies memorization and generalization in generative models. A common hypothesis is that diffusion models learn a distribution where each training sample is the center of a mode [14, 15, 16, 17, 18]. Generalization then occurs when the capacity of the model is insufficient to memorize all training samples, or when the sampling procedure is stopped early, before each generated sample has collapsed onto one of the modes. However, it is unclear how such a multimodal solution is learned dynamically, especially in the presence of architectural constraints and regularization. Here, we consider a unimodal learned distribution instead, and predict how it is learned from samples. The dynamics of learning have been studied in [19], who predict precise learning curves for random feature models, finding that generalization occurs when N is on the order of the number of features. Li et al. [20] have highlighted the importance of early stopping in training one-layer diffusion models, asserting that when optimally stopped, the Kullback-Leibler divergence scales at most with $N^{-2/5}$ and the model capacity for unimodal distributions. However, it is not yet clear how learning outcomes are related to the structure in the data distributions. Favero et al. [21] assume that ρ is a random hierarchy model [22], and assert that diffusion models generalize when N is polynomial in d . Other works have assessed that if the data lie on a lower-dimensional manifold, the required number of samples scales exponentially [23, 15] or linearly [24] with the dimension of the manifold, rather than the embedding dimension. The authors of [25] establish the first results on linear diffusion models, asserting that generalization measures on Σ, Σ_0 converge at N linear or quadratic in d , depending on whether the measure concerns the eigenvalues or also the eigenvectors of the matrices. Our work can include the case of a lower-dimensional manifold (by setting Σ to be a low-rank matrix). In contrast to the above, we predict readily measurable quantities such as the test and training loss and their dependence on N , the training dynamics and regularization.

2 Diffusion Models

In this section, we will provide a short introduction to diffusion models based on [3, 26]. Diffusion models consist of an iterative noising and denoising process. The noising process simplifies the distribution of a sample x_0 from ρ through the addition of noise

$$x_t = \sqrt{1 - \beta_t}x_{t-1} + \sqrt{\beta_t}\epsilon, \quad \epsilon \sim \mathcal{N}(0, \text{Id})$$

for a number of noising steps $t \in \{1, \dots, T\}$ and $\beta_t \in (0, 1)$, typically $\beta_t < 1$ and $T \sim 10^3$. As t increases, the original signal x_0 is gradually suppressed compared to the isotropic Gaussian noise, until one obtains x_T whose distribution is assumed to be close to $\mathcal{N}(0, \text{Id})$. Defining $\alpha_t = 1 - \beta_t$ and $\bar{\alpha}_t = \prod_{s>0}^t \alpha_s$ one can achieve the noising process up to t in a single step

$$x_t(\epsilon_t) = \sqrt{\bar{\alpha}_t}x_0 + \sqrt{1 - \bar{\alpha}_t}\epsilon_t, \quad \epsilon_t \sim \mathcal{N}(0, \text{Id}), \quad (1)$$

which enables an efficient implementation of the noising process.

Diffusion models are optimized to reverse the noising process: they implement a mapping $\epsilon_\theta(x_t, t)$ whose parameters θ are optimized to predict the noise vector ϵ_t . For a dataset \mathcal{D} consisting of N samples in \mathbb{R}^d , this amounts to minimizing

$$L = \frac{1}{dT|\mathcal{D}|} \sum_t \sum_{x_0 \in \mathcal{D}} \mathbb{E}_{\epsilon_t} \|\epsilon_t - \epsilon_\theta(x_t(\epsilon_t), t)\|^2, \quad (2)$$

which we will refer to as the (training) loss. Once trained, the denoiser is then used to iteratively generate new samples. The generation process follows the reverse direction to the noising process, starting from pure white noise $u_0 \sim \mathcal{N}(0, \text{Id})$ and culminating in a new sample u_T . For sampling, we will use $s = T - t$ as an iteration index and u as a dynamical variable to distinguish the noising process from the denoising process. The iteration reads

$$u_{s+1} = \mu_\theta(u_s, T - s) + \sigma_{T-s}\xi, \quad \xi \sim \mathcal{N}(0, \text{Id}). \quad (3)$$

where we defined

$$\mu_\theta(x_t, t) := \frac{x_t - \sqrt{1 - \bar{\alpha}_t \epsilon_\theta(x_t, t)}}{\sqrt{\bar{\alpha}_t}} + \sqrt{(1 - \sigma_t^2) - \bar{\alpha}_{t-1} \epsilon_\theta(x_t, t)} . \quad (4)$$

These two equations can be understood as first predicting $x_0 \approx \frac{x_t - \sqrt{1 - \bar{\alpha}_t \epsilon_\theta}}{\sqrt{\bar{\alpha}_t}}$, then adding back "noise" in the form of $\sigma_t \xi + \sqrt{(1 - \sigma_t^2) - \bar{\alpha}_{t-1} \epsilon_\theta}$.

2.1 Affine linear denoisers

Typical architectures for ϵ_θ are very complex, including U-nets [27] and transformers. To build a theory of diffusion models, we instead focus on linear denoisers. Linear neural networks [28, 29] have a long history of successfully elucidating various phenomena in machine learning theory, such as the double descent phenomenon [12] or the dynamics of learning semantic information [30]. Here, we consider the case where for each t , the denoiser is implemented by an affine linear mapping

$$\epsilon_\theta(x_t, t) = W_t(x_t - \sqrt{\bar{\alpha}_t} b_t) \quad (5)$$

where $W_t \in \mathbb{R}^{d \times d}$ is a weight matrix and $b_t \in \mathbb{R}^d$ a bias term. Training the denoiser then amounts to optimizing eq. (2) with respect to $\{W_t, b_t\}_t$. We will also add a standard regularization term $\sum_t \gamma_t \text{Tr } W_t W_t^\top$ to the training objective, where the prefactor γ_t allows us to apply different levels of regularization to different noising stages t . With these definitions in hand, we now move to our first results on the generalization abilities of linear diffusion models.

3 Optimal linear diffusion models on unstructured data

In this section, we will explore the general mechanisms underlying generalization with N in the linear case. Ultimately, we will compute the Kullback-Leibler divergence, which compares the distribution of the samples from the model to the ground truth. However, in practice, this quantity is often not accessible. Hence, we will first characterize the test loss, as it is readily measured also in the case of non-linear models and non-Gaussian data. We then make a connection between these two quantities, highlighting that they both penalize the absence of relevant directions of variation in the training data at small N .

Since W_t, b_t are not coupled in eq. (2) across different values of t , we can find their optima independently for each noising stage. Inserting eq. (5) into eq. (2), we find that the contribution for each t decomposes into a data-dependent term and one which depends only on the additive noise

$$\mathbb{E}_{\epsilon_t} \|\epsilon_t - \epsilon_\theta(x_t, t)\|^2 = \bar{\alpha}_t \|W_t(x_0 - b_t)\|^2 + \mathbb{E}_{\epsilon_t} \|(1 - \sqrt{1 - \bar{\alpha}_t} W_t) \epsilon_t\|^2 . \quad (6)$$

We will not consider variations which arise due to the fact that only a finite number of noised samples are used at each training step, hence in eq. (6) we take the average over infinitely many realizations of ϵ_t .

Eq. (6) shows that the loss contains only terms either linear or quadratic in the training data x_0 . Consequently, only the first two moments of the data will contribute to eq. (2). We therefore define the empirical mean μ_0 and covariance Σ_0

$$\mu_0 := \frac{1}{N} \sum_{x_0 \in \mathcal{D}} x_0 , \quad \Sigma_0 := \frac{1}{N} \sum_{x_0 \in \mathcal{D}} (x_0 - \mu_0)(x_0 - \mu_0)^\top . \quad (7)$$

To evaluate the minimum of the training loss, we add the regularization term $\sum_t \gamma_t \text{Tr } W_t W_t^\top$ to the loss and evaluate both the average over ϵ_t and the sum over the data set. Eq. (6) is quadratic in W_t, b_t , hence it is convex with the unique minimum

$$b_t^* = \mu_0 , \quad W_t^* = \frac{\sqrt{1 - \bar{\alpha}_t}}{\bar{\alpha}_t \Sigma_0 + (1 - \bar{\alpha}_t + \gamma_t) \text{Id}} . \quad (8)$$

3.1 Test and residual loss

Using eq. (8), we now evaluate the difference between the the optimal training loss and the test loss, where the average runs over ρ instead of the training data. This will help us understand how the mapping obtained from finite N performs compared to the optimal linear denoiser, the reference model we expect or architecture to converge to.

To understand how test and training loss evolve as we vary N , we express both quantities using the spectral properties of Σ_0 . Since Σ_0 is real and symmetric, it has an eigendecomposition $\Sigma_0 = \sum_{\nu} \lambda_{\nu}^0 e_{\nu}^0 \otimes e_{\nu}^0$, with $\{\lambda_{\nu}^0\}_{\nu}$ its eigenvalues, $\{e_{\nu}^0\}_{\nu}$ its normalized eigenvectors and \otimes the outer product. At the optimum, W_t^*, b_t^* , we find the irreducible, or residual, loss

$$R = \sum_t \sum_{\nu} \left[\frac{\bar{\alpha}_t \lambda_{\nu}^0 + \gamma_t}{(\bar{\alpha}_t \lambda_{\nu}^0 + (1 - \bar{\alpha}_t + \gamma_t))} \right]. \quad (9)$$

which is the minimal value of the training loss which a linear denoiser can achieve. Since the test loss is a quadratic function of the data, the only statistics of ρ needed to evaluate it are the population mean μ and the population covariance Σ .

Using the shorthand notation $\Sigma_{\mu, \nu} = (e_{\mu}^0)^T \Sigma e_{\nu}^0$ for the entries of Σ in the eigenbasis of Σ_0 , we find the difference between R and the test loss

$$L_{\text{test}} - R = \sum_t (\bar{\alpha}_t - \bar{\alpha}_t^2) \sum_{\nu} \left[\frac{\Sigma_{\nu\nu} - \lambda_{\nu}^0}{(\bar{\alpha}_t \lambda_{\nu}^0 + (1 - \bar{\alpha}_t + \gamma_t))^2} + \frac{(\mu - \mu_0)_{\nu}^2}{(\bar{\alpha}_t \lambda_{\nu}^0 + (1 - \bar{\alpha}_t + \gamma_t))^2} \right]. \quad (10)$$

Eq. (10) shows explicitly that the gap between R and L_{test} arises whenever there is a mismatch between μ_0 , Σ_0 and μ , Σ . The terms that contribute the most strongly to $L_{\text{test}} - R$ are those for which the denominator under the sum is minimized. This occurs for the smallest values of λ_{ν} and the smallest values of t , as there $1 - \bar{\alpha}_t$ is minimized. When the number of data in the training set, N , is smaller than the dimension d , at least $N - d$ eigenvalues of Σ_0 are exactly zero, giving rise to large contributions in eq. (10).

In fig. 2 we exemplify the overfitting phenomenon using a standard normal distribution $\rho = \mathcal{N}(0, \text{Id})$. We average over draws of the training data using the Marčenko-Pastur law [31] which predicts the spectral density of Σ_0 in the $N, d \rightarrow \infty, N/d = \text{const.}$ limit. We show examples of the Marčenko-Pastur distribution for several values of $\frac{N}{d}$ in fig. 2. For $N < d$, the distribution acquires a Dirac delta peak at $\lambda_0 = 0$ corresponding to the nullspace of Σ_0 and a bulk of non-zero eigenvalues. As $\frac{N}{d}$ increases above one, the delta peak vanishes and the bulk eventually concentrates around 1.

The presence of zero eigenvalues in the spectrum of Σ_0 is reflected in a very large gap between training and test loss in fig. 2 b) when $N < d$. However, this gap can effectively be reduced by regularization, through the presence of γ_t in the denominator of 10. A promising choice is $\gamma_t = \bar{\alpha}_t c$, with $c \in \mathbb{R}, c > 0$, which regularizes the denoiser for lower t more strongly than for larger t , befitting our earlier observation that overfitting is most severe at small t . In 2 we see that even minor levels ($c = 0.01$) of regularization significantly reduce overfitting. This choice of γ_t corresponds to replacing Σ_0 in eq. (8) by $\bar{\alpha}_t \Sigma_0^{\text{eff}}$, where $\Sigma_0^{\text{eff}} = \Sigma_0 + c \text{Id}$ is an effective covariance matrix. Therefore, one can interpret the presence of a regularization term as an assumption on the minimal level of variability c in an arbitrary direction. On the other hand, we can see it as a cutoff imposed on the eigenvalues of Σ_0 , below which the structure of the distribution of ρ_N cannot be resolved.

3.2 Sample statistics at the optimum

In the previous section, we have compared empirically accessible quantities such as test and training loss. Now, we move to a measure which directly compares the distributions of the generated samples and ρ , the Kullback-Leibler divergence (DKL).

Affine linear denoisers sample from Gaussian distributions: Starting from an initial Gaussian random variable $u_0 \sim \mathcal{N}(0, \text{Id})$, u_T is a linear map of Gaussian random variables and constants, hence it is also Gaussian. Up to orders of T^{-1} , affine linear networks reproduce the mean μ_0 and covariance Σ_0 of

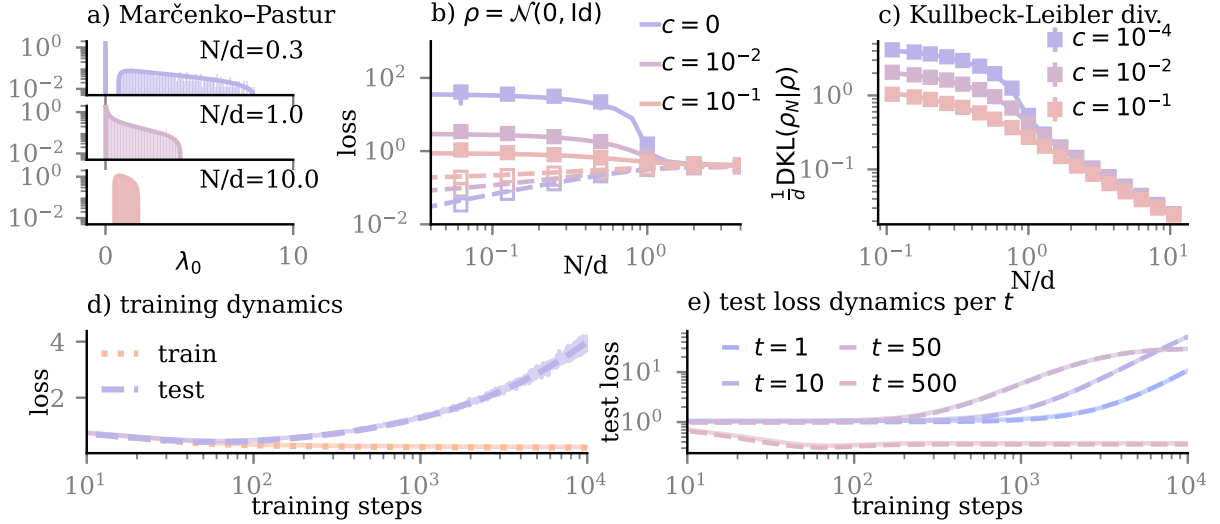


Figure 2: a) Marčenko-Pastur distribution for varying fractions N/d . b) Prediction for test loss (full lines) and residual loss (dashed lines) over N/d . Empty symbols are simulation results for the residual loss, full symbols denote the test loss, averaged over 5 random draws of training sets per data point. c) Kullback-Leibler divergence between sampling distribution and ρ . Lines are prediction, squares report averages over 10 draws of the data. d) Training and test loss over training steps for one draw of the training data in addition to prediction (dashed lines) for $N/d = 0.5$ and $c = 0$. e) Same as d), but per denoising step t . All results were obtained for $\rho = \mathcal{N}(0, \text{Id})$ and $d = 2^6$. Error bars for simulation results report one standard deviation.

the training data (for a derivation, see appendix C.3). Consequently, the distribution of samples from the linear denoiser is $\rho_N = \mathcal{N}(\mu_0, \Sigma_0 + c\text{Id})$, where c is a small parameter. The presence of c can be interpreted as originating either from the corrections due to the finite number of sampling steps (see appendix C for details), or from the regularization term $\gamma_t = \sqrt{\bar{\alpha}_t}c$.

We now impose a Gaussian hypothesis on the data $\rho = \mathcal{N}(\mu, \Sigma)$. This assumption lets us treat exclusively the deviations between ρ, ρ_N which arise due to finite N , because ρ is in principle reachable with a linear denoiser (opposed to non-Gaussian distributions). To characterize the deviations due to finite N , we compute the DKL between the distribution of samples and ρ

$$\text{DKL}(\rho_N|\rho) = \frac{1}{2} \left[\ln \frac{|\Sigma|}{|\Sigma_0 + c\text{Id}|} + (\mu - \mu_0)^T \Sigma^{-1} (\mu - \mu_0) + \text{Tr} \Sigma^{-1} (\Sigma_0 + c\text{Id}) - d \right], \quad (11)$$

which is a measure of distance between distributions, in particular $\text{DKL}(\rho'|\rho) = 0 \Leftrightarrow \rho' = \rho$. The most dominant term at small N is $\text{DKL}(\rho_N|\rho)$ is $\ln \frac{|\Sigma|}{|\Sigma_0^{\text{eff}}|} = \sum_{\nu} \ln \frac{\lambda_{\nu}}{\lambda_{\nu}^0 + c}$, where λ_{ν} are the eigenvalues of Σ . This term in the DKL heavily penalizes the presence of a nullspace in Σ_0 for small c , analogous to the test loss.

We show the DKL in 2c) finding the same two relevant regimes as in the test loss: first, when $N < d$, regularization is effective to reduce the Kullback-Leibler divergence. Second, when $N > d$, the $\text{DKL}(\rho_N|\rho)$ diminishes rapidly. This decrease in 11 not mirrored in the test loss, which plateaus due to the presence of the residual loss R .

3.3 The speed of learning

We solve the learning dynamics of matrices W_t for centered datasets ($\mu_0 = 0$) in appendix B. We find that the elements of W_t exponentially relax towards 8 at a different rates $\bar{\alpha}_t \lambda_{\nu}^0 + 1 - \bar{\alpha}_t + \gamma_t$ corresponding to different spatial directions. The rate $\bar{\alpha}_t \lambda_{\nu}^0 + 1 - \bar{\alpha}_t + \gamma_t$ corresponds precisely to the denominator of the terms in eq. (10), whose minimal values lead to the most severe overfitting. This means that the

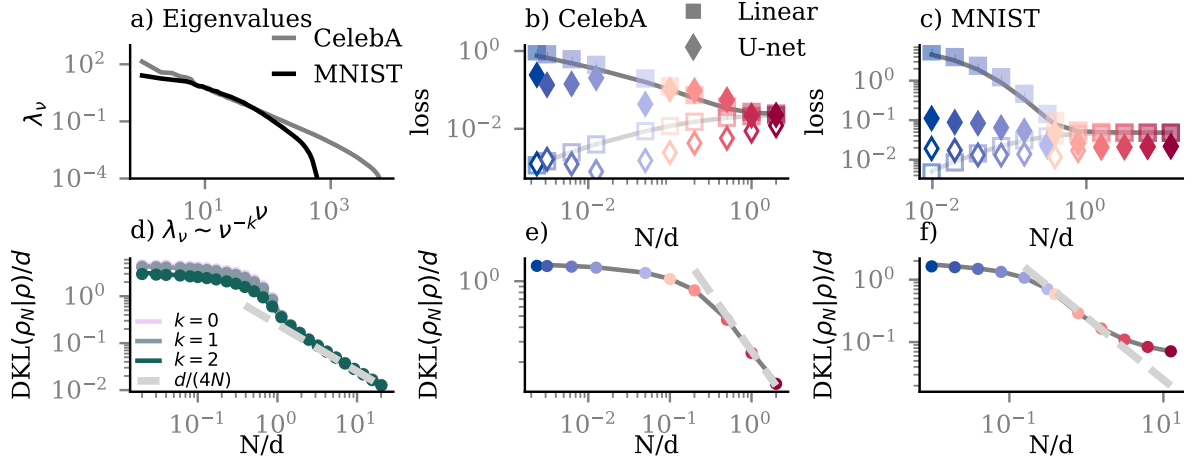


Figure 3: a) Eigenvalues of CelebA and MNIST dataset, sorted by rank. b) and c) show test loss (filled symbols simulation, dark gray curves prediction) and training loss (empty symbols simulation, light gray curves prediction) for over number of training samples. In the linear case, test and training loss are averaged over Gaussian samples with the same mean and covariance as the data, averaged over 100 draws of the training set. In the nonlinear case, they are averaged over $\min\{100, N\}$ training and 200 test samples. d) Kullback-Leibler divergence between sample distribution of linear diffusion models with regularization $c = 10^{-4}$ and ρ , where the eigenvalues of Σ follow a powerlaw. Symbols are averages over 10 random draws of the training sets, error bars report one standard deviation, but are typically smaller than the symbol size. e) and f) are equivalent to d), but for Σ originating from the CelebA and MNIST datasets, respectively.

most precarious directions in the sense of overfitting are also the ones which are learned the slowest. At the same time, regularization speeds up the learning process in all directions, as it increases the rate of convergence to the optimum. We compare our analytical results to the training curves of linear neural networks in fig. 2 d). While the training loss approaches R exponentially, we see that the test loss initially decays, then increases again, as the model overfits the data. Furthermore, we see in fig. 2 d) that, the smaller t is, the later overfitting occurs. This makes early stopping an effective strategy to prevent overfitting.

Throughout this section, we have considered the case of $\Sigma = \text{Id}$. For realistic data, we must treat the case of general Σ , which we will do in the following.

4 Structured data

To move towards a more realistic model of data, we now consider two widely used image-datasets: the CelebA dataset [11], a dataset of celebrity portraits, down-sampled to 80×80 grayscale pixels, and the MNIST dataset, a dataset of handwritten digits [32], up-sampled to 32×32 pixels. We provide the code used to produce these results in [33].

Recall that for linear diffusion models, the relevant structure of ρ enters via the mean μ and its covariance Σ . For many realistic datasets, including CelebA and MNIST, we find that the spectra of Σ are strongly hierarchical, meaning that there are few eigendirections with large variance and many eigendirections with comparatively small variance, see fig. 3a). This hierarchy in the eigenvalues can be quantified e.g. using the participation ratio, $D_{PR} = \frac{(\text{Tr } \Sigma)^2}{\text{Tr } \Sigma^2}$, a measure of effective dimensionality. For example, for the CelebA dataset, $d = 6400$, but $D_{PR} \approx 7.8$, in the MNIST dataset, we find $d = 1024$, but $D_{PR} \approx 25$.

To evaluate the test loss or the Kullback-Leibler divergence, we must average over the different realizations of Σ_0 originating from independent draws of the data from ρ . This is far from straightforward, as the random matrix Σ_0 appears e.g. in the denominator of the test loss. In appendix D, we

use the replica trick to compute a potential whose derivatives create the necessary averages. The use of this trick dates back to [34], and has been used e.g. to compute the spectra of sparse random matrices [35, 36]. We find that the averages depend on a quantity q which must be determined self-consistently from the spectrum of Σ . We will express our result using q and the weighted sum $R_k(q)$, which are determined by

$$q_t = \frac{1}{d} \sum_{\nu} \frac{\lambda_{\nu}}{1 + \lambda_{\nu} \frac{\hat{\alpha}_t N}{d q \hat{\alpha}_t + N d}} \quad R_k^t = d^{-1} \sum_{\nu} \frac{\lambda_{\nu}^k}{\left(q_t + \frac{N}{d \hat{\alpha}_t} + \frac{N}{d} \lambda_{\nu}\right)^2}. \quad (12)$$

where $\hat{\alpha}_t = \bar{\alpha}_t / (1 - \bar{\alpha}_t + \gamma_t)$.

4.1 Test loss

Using eq. (12) we can then express the test loss via

$$L_{\text{test}} = 1 + \frac{1}{T} \sum_t \frac{1}{1 + \frac{\gamma_t}{1 - \bar{\alpha}_t}} \left[\frac{(q_t + \frac{N}{d \hat{\alpha}_t})^2}{1 - \bar{\alpha}_t + \gamma_t} \left(R_0^t + R_1^t + \frac{(R_2^t)^2 + (R_1^t)^2}{1 - \frac{N}{d} R_2^t} \right) - \frac{2}{d} \text{Tr} \frac{\text{Id}}{\text{Id} + \frac{N \hat{\alpha}_t}{d \hat{\alpha}_t q_t + N} \Sigma} \right] \quad (13)$$

In fig. 3, we compare test and training loss computed using both linear models at the optimum eq. (8) and nonlinear models. While the data points originating from the nonlinear models are in general more noisy and do not follow the trajectory of the linear models, we find that the gap between the training and test closes approximately at the same number of training data. For the MNIST data, the test loss computed on different architectures does not converge to the same value, with the U-net architecture outperforming the linear model. While the U-net architecture is far more flexible and is expected to outperform the linear model, we believe that this deviation is mostly due to the MNIST data being almost binary: almost all pixels in the MNIST images saturate to either $+1$ or -1 , meaning that a non-linear model which predicts the noise to be the difference to the closest binary variable will naturally outperform a linear model.

4.2 Alignment with the reference model

While the test loss is readily evaluated across datasets and architectures, it plateaus when $N > d$, even when other generalization measures, such as the Kullback-Leibler divergence, continue to improve. We hence define the following measure, which does not saturate in this regime

$$\Delta \epsilon_N = \frac{1}{T} \sum_t \langle ||\epsilon_N(x^{\text{test}}) - \epsilon_{\infty}(x^{\text{test}})_t||^2 \rangle_{(x^{\text{test}})},$$

where (x^{test}) are noised test samples, ϵ_N is the mapping obtained from a finite dataset of N samples and ϵ_{∞} is the mapping obtained from an infinite number of samples. In practice, when only finite number of data are available, we choose ϵ_{∞} as the mapping optimized on the largest subset of the data. $\Delta \epsilon_N$, obtained from disjoint data sets, then measures if the mapping has generalized towards a solution which is independent of the training set. For linear diffusion models, we find

$$\Delta \epsilon_N = L_{\text{test}} - 1 + \frac{1}{T} \sum_t \frac{1 - \bar{\alpha}_t}{(1 - \bar{\alpha}_t + \gamma_t)} \text{Tr} (\text{Id} + \hat{\alpha}_t \Sigma)^{-1}. \quad (14)$$

Note the similarity between $\Delta \epsilon_N$ and the test loss eq. (13): these two measures differ only by terms independent of N , which are responsible for the plateau of the test loss. In the unsaturated regime, the test loss is a good proxy for $\Delta \epsilon_N$. For $N > d$, increasing N continues to improve generalization (measured by $\Delta \epsilon_N$), but this effect is no longer reflected in the test loss. In fig. 1 a), we show $\Delta \epsilon_N$ for the CelebA dataset, both for linear and non-linear diffusion models, as well as a prediction in the average over draws of the dataset from replica theory. We find that both for linear and non-linear diffusion models, the curves show a kink around $N \sim 10^3$, which is precisely where the gap between training and test loss closes (see fig. 2 c)) and memorization diminishes (see fig. 1 d)).

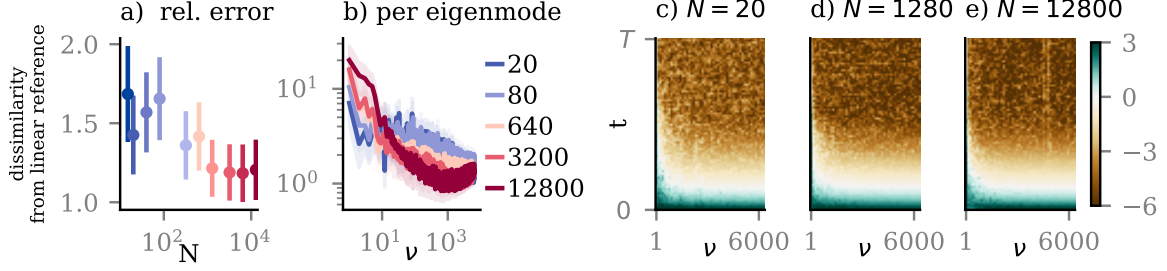


Figure 4: Relative difference of non-linear denoisers from best linear model, per noising step t and direction ν , trained on increasing numbers of data. a) averaged over ν and t , b) averaged over t , c) - e) $\log d_{t,\nu}$ per ν, t . All data are averaged over 100 test samples per t, ν .

4.3 Kullback-Leibler divergence

As a final measure of generalization, we compare the Kullback-Leibler divergence between our Gaussian hypothesis on the data $\rho = \mathcal{N}(\mu, \Sigma)$ and the sampling distribution $\rho_N = \mathcal{N}(\mu_0, \Sigma_0 + c\text{Id})$. We then find

$$\begin{aligned} \frac{1}{d} \text{DKL}(\rho_N | \rho) = & \frac{1}{2} \frac{\frac{q}{c}}{\frac{d}{Nc}q + 1} - \frac{1}{2d} \sum_i \ln \left| \frac{c}{\lambda_i} + \frac{1}{\frac{d}{Nc}q + 1} \right| - \frac{N}{2d} \ln \left(\frac{d}{Nc}q + 1 \right) \\ & + \frac{d + 2\sqrt{c} \text{Tr} \Sigma^{-\frac{1}{2}} + c \text{Tr} \Sigma^{-1}}{2Nd} + \frac{c}{2d} \text{Tr} \Sigma^{-1} \end{aligned} \quad (15)$$

where the first line in eq. (15) originates from the term $\ln |\Sigma|/|\Sigma_0 + c\text{Id}|$ and q is computed from 12 with $\hat{\alpha}_t = c^{-1}$. When c is very small, the terms in the first line eq. (15) dominate the expression. In fig. 3 d) e), f) we compare measurements of $\text{DKL}(\rho_N | \rho)$ to the outcome of eq. (15) for Σ measured on MNIST and CelebA, and case where the eigenvalues of Σ are follow a power-law. Analogously to the case of unstructured data, the first line of eq. (15) penalizes the presence of a nullspace of Σ_0 , although this can be mediated by the presence of very small eigenvalues in Σ . For $N < d$, the presence of a hierarchy in the eigenvalues of Σ (controlled e. g. by increasing k in fig. 3d)) can decrease the DKL. Intuitively, this is because the absence of variation in Σ_0 is not as significant when the corresponding variation in Σ is also small. We find that for $N > d$, the DKL collapses on to the same line independently of the specifics of Σ . The independence of the DKL on Σ has been noted in [37], who argued that this makes the DKL a good measure for the similarity of Σ_0 to Σ . In D.8, we show that when c is much smaller than the smallest eigenvalue of Σ and $N > d$ the DKL is approximately given by $d/(4N)$, where we have neglected terms of order $(d/N)^2$ and \sqrt{c} . In the $N > d$ regime, we find this scaling of the DKL across realizations of Σ (see fig. 3 d) - f)), up to deviations which originate from $c > 0$, which causes a saturation of the DKL above zero.

5 Differences between linear and non-linear models

We now test whether the mappings encoded by different architectures are indeed similar. Prior studies have observed increasing similarity between non-linear and linear models with t , see [38, 39]. We compute the relative distance of their mappings in the eigenspace of Σ . We define a direction - and t dependent distance $d_{t,\nu}$ measure

$$d_{t,\nu} = \frac{(\epsilon^N(x_t, t) - \epsilon_\infty^*(x_t, t))_\nu^2}{|\epsilon^N(x_t, t) + \eta|_\nu |\epsilon_\infty^*(x_t, t) + \eta|_\nu} \quad (16)$$

where ϵ^N is a U-net trained on N examples and ϵ_∞^* is a linear model with modest regularization $c = 10^{-2}$, trained on the maximal amount of available data and $\eta = 10^{-3}$ prevents divergences. In fig. 4, we show $d_{t,\nu}$ for the CelebA dataset. Overall, we find that the relative error decays with N, ν and t . Indeed for a large extent of t, ν , the difference between linear and non-linear models becomes very

small. However, for leading eigenmodes (small ν), the differences between linear and non-linear models grow with N . This (small ν , small t) is also the regime where we expect the non-Gaussianity of the data to have the largest effect.

6 Discussion

We have identified two relevant regimes for generalization in linear diffusion models, $N > d$ and $N < d$. When $N < d$, the model overfits due to a lack of variability in the training set, namely the low-rank structure of the empirical covariance matrix. Both the Kullback-Leibler divergence and test loss strongly penalize this lack of variability. However, overfitting can be mitigated by applying early stopping and regularization. Regularization acts both as a prior on the minimal amount of variability in any direction of the data and as a cutoff on the spectrum of Σ below which the structure of the distribution cannot be resolved. For $N > d$, structure in the data plays a minor role and generalization measured by the Kullback-Leibler divergence decays linearly with d/N , even for data which are believed to be intrinsically low-dimensional.

Intriguingly, we found that a highly hierarchical structure in the data usually associated with a lower effective dimensionality has no significant effect on the emergence of the two regimes. This suggests that linear diffusion models place emphasis on learning all directions with finite variability, not only those with the highest levels of variation. A similar effect has previously been observed in [40], where learning in the supervised setting was contrasted with diffusion models. In the supervised case, an effect called benign overfitting occurs: if the data consist of a signal that is corrupted by noise, the model may overfit to the signal, ignoring the noise. In diffusion models, however, both the signal and the noise are faithfully represented, meaning that all variability in the data is taken into account. This is intuitive, given that the objective in training diffusion models is precisely to draw from a distribution with the same level of variability.

One important open issue remains to identify the “correct” metric to measure generalization in diffusion models. The authors of [25] have argued that even for linear models, the relevant scaling of N with d is either linear (as in the Kullback-Leibler divergence considered here) or quadratic, depending on the metric. Nevertheless, the practical consequences we draw from our analysis are simple: When $N < d$, then either regularization or early stopping are effective to prevent overfitting, whereas $N > d$ is naturally favored.

Finally, we found that linear diffusion models are very similar to their non-linear counterparts in a significant portion of the sampling trajectory and data space. Accounting for the non-linearity of the mapping especially for leading eigendirections of Σ and low levels of noise will be a fruitful direction of future research.

Acknowledgements

We are grateful to Alessio Giorlandino for helpful discussions. CM and SG gratefully acknowledge funding from Next Generation EU, in the context of the National Recovery and Resilience Plan, Investment PE1 – Project FAIR “Future Artificial Intelligence Research” (CUP G53C22000440006). SG additionally acknowledges funding from the European Research Council (ERC) for the project “beyond2”, ID 101166056, and from the European Union–NextGenerationEU, in the framework of the PRIN Project SELF-MADE (code 2022E3WYTY – CUP G53D23000780001).

References

- [1] Jascha Sohl-Dickstein, Eric A Weiss, Niru Maheswaranathan, and Surya Ganguli. Deep Unsupervised Learning using Nonequilibrium Thermodynamics.
- [2] Yang Song and Stefano Ermon. Generative Modeling by Estimating Gradients of the Data Distribution. In *Advances in Neural Information Processing Systems*, volume 32. Curran Associates, Inc., 2019.
- [3] Jonathan Ho, Ajay Jain, and Pieter Abbeel. Denoising Diffusion Probabilistic Models, December 2020. arXiv:2006.11239 [cs, stat].
- [4] Valentin De Bortoli, James Thornton, Jeremy Heng, and Arnaud Doucet. Diffusion Schrödinger Bridge with Applications to Score-Based Generative Modeling. In *Advances in Neural Information Processing Systems*, volume 34, pages 17695–17709. Curran Associates, Inc., 2021.
- [5] Adam Block, Youssef Mroueh, and Alexander Rakhlin. Generative Modeling with Denoising Auto-Encoders and Langevin Sampling, October 2022. arXiv:2002.00107 [stat].
- [6] Valentin De Bortoli. Convergence of denoising diffusion models under the manifold hypothesis, May 2023. arXiv:2208.05314 [stat].
- [7] Xingchao Liu, Lemeng Wu, Mao Ye, and Qiang Liu. Let us Build Bridges: Understanding and Extending Diffusion Generative Models, August 2022. arXiv:2208.14699 [cs].
- [8] Holden Lee, Holden Lee, Jhu Edu, Jianfeng Lu, Yixin Tan, and Yixin Tan. Convergence of score-based generative modeling for general data distributions.
- [9] Jakiw Pidstrigach. Score-Based Generative Models Detect Manifolds, October 2022. arXiv:2206.01018 [stat].
- [10] Zahra Kadkhodaie, Florentin Guth, Eero P. Simoncelli, and Stéphane Mallat. Generalization in diffusion models arises from geometry-adaptive harmonic representations, April 2024. arXiv:2310.02557 [cs].
- [11] Ziwei Liu, Ping Luo, Xiaogang Wang, and Xiaoou Tang. Deep Learning Face Attributes in the Wild. pages 3730–3738. IEEE Computer Society, December 2015. ISSN: 2380-7504.
- [12] Madhu S Advani, Andrew M Saxe, and Haim Sompolinsky. High-dimensional dynamics of generalization error in neural networks. *Neural Networks*, 132:428–446, 2020.
- [13] Kirsten Fischer, Alexandre René, Christian Keup, Moritz Layer, David Dahmen, and Moritz Helias. Decomposing neural networks as mappings of correlation functions. *Physical Review Research*, 4(4):043143, November 2022. Publisher: American Physical Society.
- [14] Luca Ambrogioni. In search of dispersed memories: Generative diffusion models are associative memory networks, November 2023. arXiv:2309.17290 [cs, stat].
- [15] Beatrice Achilli, Luca Ambrogioni, Carlo Lucibello, Marc Mézard, and Enrico Ventura. Memorization and Generalization in Generative Diffusion under the Manifold Hypothesis, February 2025. arXiv:2502.09578 [cond-mat].
- [16] Giulio Biroli, Tony Bonnaire, Valentin de Bortoli, and Marc Mézard. Dynamical Regimes of Diffusion Models, February 2024. arXiv:2402.18491 [cond-mat].
- [17] Anand Jerry George, Rodrigo Veiga, and Nicolas Macris. Analysis of Diffusion Models for Manifold Data, February 2025. arXiv:2502.04339 [math].

- [18] Bao Pham, Gabriel Raya, Matteo Negri, Mohammed J. Zaki, Luca Ambrogioni, and Dmitry Krotov. Memorization to Generalization: The Emergence of Diffusion Models from Associative Memory. November 2024.
- [19] Anand Jerry George, Rodrigo Veiga, and Nicolas Macris. Denoising Score Matching with Random Features: Insights on Diffusion Models from Precise Learning Curves, February 2025. arXiv:2502.00336 [cs].
- [20] Puheng Li, Zhong Li, Huishuai Zhang, and Jiang Bian. On the Generalization Properties of Diffusion Models, March 2025. arXiv:2311.01797 [cs].
- [21] Alessandro Favero, Antonio Sclocchi, Francesco Cagnetta, Pascal Frossard, and Matthieu Wyart. How compositional generalization and creativity improve as diffusion models are trained, March 2025. arXiv:2502.12089 [stat].
- [22] Francesco Cagnetta, Leonardo Petrini, Umberto M. Tomasini, Alessandro Favero, and Matthieu Wyart. How Deep Neural Networks Learn Compositional Data: The Random Hierarchy Model. *Physical Review X*, 14(3):031001, July 2024. Publisher: American Physical Society.
- [23] Minshuo Chen, Kaixuan Huang, Tuo Zhao, and Mengdi Wang. Score Approximation, Estimation and Distribution Recovery of Diffusion Models on Low-Dimensional Data. *ArXiv*, abs/2302.07194:null, 2023.
- [24] Peng Wang, Huijie Zhang, Zekai Zhang, Siyi Chen, Yi Ma, and Qing Qu. Diffusion Models Learn Low-Dimensional Distributions via Subspace Clustering, December 2024. arXiv:2409.02426 [cs].
- [25] Giulio Biroli and Marc Mézard. Generative diffusion in very large dimensions. *Journal of Statistical Mechanics: Theory and Experiment*, 2023(9):093402, September 2023.
- [26] Jiaming Song, Chenlin Meng, and Stefano Ermon. Denoising Diffusion Implicit Models, October 2022. arXiv:2010.02502.
- [27] Olaf Ronneberger, Philipp Fischer, and Thomas Brox. U-Net: Convolutional Networks for Biomedical Image Segmentation, May 2015. arXiv:1505.04597 [cs].
- [28] Pierre Baldi and Kurt Hornik. Neural networks and principal component analysis: Learning from examples without local minima. *Neural networks*, 2(1):53–58, 1989.
- [29] Andrew M Saxe, James L McClelland, and Surya Ganguli. Exact solutions to the nonlinear dynamics of learning in deep linear neural networks. In *ICLR*, 2014.
- [30] Andrew M Saxe, James L McClelland, and Surya Ganguli. A mathematical theory of semantic development in deep neural networks. *Proceedings of the National Academy of Sciences*, 116(23):11537–11546, 2019.
- [31] V A Marčenko and L A Pastur. DISTRIBUTION OF EIGENVALUES FOR SOME SETS OF RANDOM MATRICES. *Mathematics of the USSR-Sbornik*, 1(4):457–483, April 1967.
- [32] Li Deng. The MNIST Database of Handwritten Digit Images for Machine Learning Research [Best of the Web]. *IEEE Signal Processing Magazine*, 29(6):141–142, November 2012.
- [33] Claudia Merger and Sebastian Goldt. Code for Generalization Dynamics of Linear Diffusion models, May 2025.
- [34] S F Edwards and R C Jones. The eigenvalue spectrum of a large symmetric random matrix. *Journal of Physics A: Mathematical and General*, 9(10):1595–1603, October 1976.

- [35] Reimer Kuehn. Spectra of Sparse Random Matrices. *Journal of Physics A: Mathematical and Theoretical*, 41(29):295002, July 2008. arXiv:0803.2886 [cond-mat].
- [36] G. J. Rodgers and A. J. Bray. Density of states of a sparse random matrix. *Physical Review B*, 37(7):3557–3562, March 1988.
- [37] Michele Tumminello, Fabrizio Lillo, and Rosario N. Mantegna. Kullback-Leibler distance as a measure of the information filtered from multivariate data. *Physical Review E*, 76(3):031123, September 2007. Publisher: American Physical Society.
- [38] Binxu Wang and John J. Vastola. The Hidden Linear Structure in Score-Based Models and its Application, November 2023. arXiv:2311.10892 [cs].
- [39] Xiang Li, Yixiang Dai, and Qing Qu. Understanding Generalizability of Diffusion Models Requires Rethinking the Hidden Gaussian Structure. November 2024.
- [40] Andi Han, Wei Huang, Yuan Cao, and Difan Zou. On the Feature Learning in Diffusion Models, December 2024. arXiv:2412.01021 [stat].

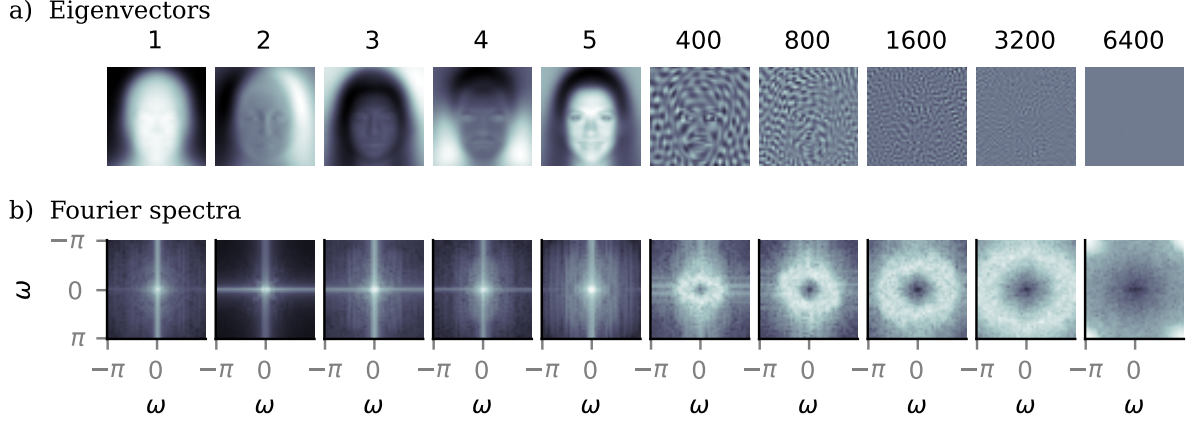


Figure A.1: a) First five leading eigenvectors $\nu = 1, \dots, 5$ of the covariance matrix of the CelebA data, as well as sub-leading eigenvectors $\nu = 400, \dots, 6400$. b) Corresponding Fourier spectra of the eigenvectors.

A A detail-based similarity measure for CelebA

For the models trained on CelebA, computing the cosine similarity $c(x, y) = \frac{x^T y}{\|x\| \|y\|}$ between a generated sample and one from the training set yields a very high similarity ~ 0.9 , even if the generated images are genuinely different. Upon manual inspection of the corresponding images, we find that this occurs due to a large portion of the image, such as the background, being uniformly dark or light.

In fig. A.1 we compare the eigenvectors of the covariance matrix of the CelebA data to their corresponding Fourier spectra. We find that leading eigenvectors $\nu = 1, \dots, 5$ have a more homogeneous spatial distribution of light and dark pixels, correspondingly their Fourier spectra are concentrated around small frequencies (small $|\omega|$). As ν increases, however, the spectra of the eigenvectors become more broad, and small frequencies are suppressed.

On the basis of these observations, we construct a similarity measure which is oriented more towards the details of the images: We first project the images into the space spanned only by sub-leading eigenvectors $\nu > 10$. We then compute the cosine similarities of the resulting vectors. We find that this measure is then more sensitive to changes in the details of the images, which leave the background uniform (e.g. for the generated image and closest training set examples in fig. 1 for $N \geq 6400$).

B Learning dynamics of linear denoisers

Throughout this section, we will assume that all data sets are centered, hence that $\mu_0 = \mu = 0$ and that the bias terms b_t are initialized at zero, corresponding to their optimal value in this case. We introduce a training time τ and a learning rate η . At each training step, we will update the parameters of the linear network θ according to

$$\theta(\tau + d\tau) - \theta(\tau) d\tau = -\eta \nabla_{\theta} L$$

We will treat the dynamics of W_t in the eigenbasis of the empirical covariance matrix,

$$W_t(\tau) = \sum_{\nu} w_{\mu, \nu, t}(\tau) e_{\mu}^0 \otimes e_{\nu}^0$$

Inserting this expression into the training loss, we find

$$L = \frac{1}{dT} \sum_t \sum_{\mu, \nu} [(\bar{\alpha}_t \lambda_{\nu}^0 + \gamma_t + 1 - \bar{\alpha}_t) w_{\mu, \nu, t}^2 - 2\sqrt{1 - \bar{\alpha}_t} w_{\mu, \nu, t}] + d$$

This expression shows that all entries in $w_{\mu,\nu,t}(\tau)$ decouple and we can treat the evolution of the weight matrices elementwise. Taking the derivative and using the definition of W_T^* (eq. (8)) we find, that in the limit $d\tau \rightarrow 0$

$$w_{\mu,\nu,t}(\tau) = w_{\mu,\nu,t}^* + \exp \left\{ -2 \frac{\eta}{dT} [\bar{\alpha}_t \lambda_\nu^0 + (1 - \bar{\alpha}_t + \gamma_t)] \tau \right\} (w_{\mu,\nu,t}(0) - w_{\mu,\nu,t}^*) . \quad (\text{B.1})$$

This expression shows that through training, the entries of W_t approach their optimal value exponentially with rate $2 \frac{\eta}{dT} [\bar{\alpha}_t \lambda_\nu^0 + (1 - \bar{\alpha}_t + \gamma_t)]$. The expression for the training and test loss, shown in 2 follows from inserting eq. (B.1) into L .

C Sampling dynamics of affine linear denoisers

In this section we compute how the mean and covariance of the samples evolve under the iterative denoising process specified in eq. (3). Before we do so, we note that to sample from a given Gaussian distribution with mean μ_0 and covariance Σ_0 , no iterative process is necessary. Rather, given $u_0 \sim \mathcal{N}(0, \text{Id})$, we can generate a sample u with the aforementioned statistics with a simple linear transform

$$u_T = \sqrt{\Sigma_0} u_0 + \mu_0 . \quad (\text{C.1})$$

we will see in the following that the iterative sampling process approaches the same statistics of u_T . In this manuscript, we do not consider the fact that the noising process is discrete, rather we will treat sampling time as continuous. However, we will highlight corrections which arise due to $\bar{\alpha}(0) \neq 1$ and $\bar{\alpha}(T) \neq 0$.

C.1 Continuous time limit

For the following calculations, it will be useful to write a continuous time version of the denoising process. To this end, we also consider a rescaled time in which the time arguments in the sampling process are incremented by $h = T^{-1}$, rather than increments of 1 as in eq. (3), thus both denoising time s and noising time t run from zero to one with $t = 1 - s$. We now assume $\beta(t) = \mathcal{O}(h)$, $\forall t$. This is reasonable, since we expect the changes in every step of the diffusion process to be small. We now define

$$\hat{\beta}(t) := \frac{\beta_t}{h} \quad \hat{\sigma}(t) := \frac{\sigma_t}{\sqrt{h}} . \quad (\text{C.2})$$

For $\bar{\alpha}(t)$, we use that $\bar{\alpha}(t+h) = (1 - \hat{\beta}(t)h) \bar{\alpha}(t)$, so in the limit $T \rightarrow \infty$, or equivalently $h \rightarrow 0$,

$$\frac{d\bar{\alpha}(t)}{dt} = -\hat{\beta}(t) \bar{\alpha}(t) . \quad (\text{C.3})$$

This differential equation admits a formal solution, namely

$$\bar{\alpha}(t) = e^{-\zeta(t)}, \zeta(t) := \int_0^t ds \hat{\beta}(s) . \quad (\text{C.4})$$

C.2 Fokker-Planck equation

With the definition of the continuous noising/denoising time limit in hand, we now write eq. (3) as a linear stochastic differential equation. We find

$$du(s) = (m(s)u(s) + c(s)) ds + \hat{\sigma}(1-s)dZ_s$$

where m_s, c_s are found by inserting eq. (4) and eq. (8) into eq. (3) and Z_s is a Wiener process. We find

$$m(s) = \frac{\hat{\beta}(1-s)}{2} \text{Id} - \frac{1}{2} \frac{(\hat{\sigma}^2(1-s) + \hat{\beta}(1-s))}{\bar{\alpha}(1-s)\Sigma_0 + (1-\bar{\alpha}(1-s))\text{Id}},$$

$$c(s) = \frac{1}{2} (\hat{\sigma}^2(1-s) + \hat{\beta}(1-s)) \frac{\sqrt{\bar{\alpha}(1-s)}}{\bar{\alpha}(1-s)\Sigma_0 + (1-\bar{\alpha}(1-s))\text{Id}} \mu_0.$$

Observe that $m(s)$ is diagonal in the eigenbasis of Σ_0 . Moving into this basis, we can now solve for the statistics of the sampling process in a decoupled manner, as in this basis, all entries of $u(s)$ are statistically independent. In the following calculation, we will keep one direction u_ν fixed, dropping the index ν for brevity. We use the Fokker-Planck equation to write down the differential equation for the density $\rho(u, t)$ which describes this variable. We have

$$\partial_s \rho(u, s) = -\partial_u [(m(s)u(s) + c(s)) \rho(u, s)] + \frac{1}{2} \partial_u^2 [\hat{\sigma}(1-s)^2 \rho(u, s)]. \quad (\text{C.5})$$

Since we know that this is a Gaussian process, we make the following Ansatz for the density

$$\rho(u, s) = \frac{1}{\sqrt{2\pi\sigma_u(s)^2}} \exp \left[-\frac{(u(s) - \mu_u(s))^2}{2\sigma_u(s)^2} \right]$$

defining $\mu_u(s), \sigma_u(s)^2$ as the mean and variance of the samples at sampling time s , respectively. With this Ansatz we find that

$$\partial_s (\sigma_u(s)^2) = 2m(s)\sigma_u(s)^2 + \hat{\sigma}(1-s)^2 \quad \partial_s \mu_u(s) = m(s)\mu_u(s) + c(s). \quad (\text{C.6})$$

which admit the solutions

$$\mu_u(s) = \exp \left(\int_0^s dv m(v) \right) \left[\int_0^s dv \exp \left(-\int_0^v dw m(w) \right) c(v) + \mu_u(0) \right] \quad (\text{C.7})$$

$$\sigma_u(s)^2 = \exp \left(2 \int_0^s dv m(v) \right) \left[\int_0^s dv \exp \left(-2 \int_0^v dw m(w) \right) \hat{\sigma}(1-v)^2 + \sigma_u(0)^2 \right] \quad (\text{C.8})$$

The initial conditions are $\sigma_u(0) = 1, \mu_u(0) = 0$ since $u(0) \sim \mathcal{N}(0, \text{Id})$. We will find closed form solutions for these integrals for two choices of $\hat{\sigma}$ in the next step.

C.3 Solutions for mean and covariance of samples

We will first simplify some of the integrals to solve these two equations. To find the variance $\sigma_u(s)^2$, we first solve

$$\int_0^s dv \hat{\beta}(1-v) = \ln \left(\frac{\bar{\alpha}(1-s)}{\bar{\alpha}(1)} \right)$$

$$\int_0^s dv \frac{-\hat{\beta}(1-v)}{\bar{\alpha}(1-v)(\lambda^0 - 1) + 1} = -\ln \left(\frac{\bar{\alpha}(1-s)}{\bar{\alpha}(1)} \right) + \ln \left(\frac{\bar{\alpha}(1-s)(\lambda^0 - 1) + 1}{\bar{\alpha}(1)(\lambda^0 - 1) + 1} \right)$$

Second, we have $c(s) = \sqrt{\bar{\alpha}(1-s)} \left(m(s) - \frac{\hat{\beta}(1-s)}{2} \right) \mu_0$. With

$$\int_0^s dv \exp \left(-\int_0^v dw m(w) \right) \sqrt{\bar{\alpha}(1-v)} \left(m(v) - \frac{\hat{\beta}(1-v)}{2} \right)$$

$$= \sqrt{\bar{\alpha}(1-s)} \exp \left(-\int_0^s dw m(w) \right) - \sqrt{\bar{\alpha}(1)}$$

we then find

$$\mu_u(s) = \sqrt{\bar{\alpha}(1-s)} \mu_0 - \exp \left(\int_0^s dv m(v) \right) \sqrt{\bar{\alpha}(1)} \mu_0$$

We now treat two different scenarios, $\hat{\sigma}^2(t) = \hat{\beta}(t)$ and $\hat{\sigma}(t) = 0$.

C.3.1 $\hat{\sigma}(t) = 0$

In this case, we have $\int_0^s dv m(v) = \frac{1}{2} \ln \left(\frac{\bar{\alpha}(1-s)(\lambda^0-1)+1}{\bar{\alpha}(1)(\lambda^0-1)+1} \right)$, hence

$$\begin{aligned}\mu_u(s) &= \sqrt{\bar{\alpha}(1-s)}\mu_0 - \sqrt{\bar{\alpha}(1) \frac{\bar{\alpha}(1-s)(\lambda^0-1)+1}{\bar{\alpha}(1)(\lambda^0-1)+1}}\mu_0 \\ \sigma_u(s)^2 &= \frac{\bar{\alpha}(1-s)(\lambda^0-1)+1}{\bar{\alpha}(1)(\lambda^0-1)+1}\end{aligned}\tag{C.9}$$

Since $\bar{\alpha}(1)$ vanishes exponentially with ζ , and $\bar{\alpha}(0) = 1 + \mathcal{O}(h)$, we find that for a long noising trajectory of many steps, $\Sigma_u = \Sigma_0 + \mathcal{O}(h)$ and $\mu_u = \mu_0 + \mathcal{O}(h)$, reproduce the empirical mean and covariance of the training set to good approximation.

C.3.2 $\hat{\sigma}^2(t) = \hat{\beta}(t)$

In this case $\int_0^s dv m(v) = \ln \left(\frac{\bar{\alpha}(1-s)(\lambda^0-1)+1}{\bar{\alpha}(1)(\lambda^0-1)+1} \right) + \frac{1}{2} \ln \left(\frac{\bar{\alpha}(1)}{\bar{\alpha}(1-s)} \right)$, hence we find the sampling mean to be

$$\mu_u(s) = \sqrt{\bar{\alpha}(1-s)}\mu_0 - \sqrt{\frac{\bar{\alpha}(1)^2}{\bar{\alpha}(1-s)} \frac{\bar{\alpha}(1-s)(\lambda^0-1)+1}{\bar{\alpha}(1)(\lambda^0-1)+1}}\mu_0.$$

To evaluate eq. (C.8) for the covariance we first solve the following integral

$$\begin{aligned}\int_0^s dv \exp \left(-2 \int_0^v dw m(w) \right) \hat{\beta}(1-v) &= \frac{(\bar{\alpha}(1)(\lambda^0-1)+1)^2}{\bar{\alpha}(1)} \\ &\cdot \left(\frac{\bar{\alpha}(1-s)}{\bar{\alpha}(1-s)(\lambda^0-1)+1} - \frac{\bar{\alpha}(1)}{\bar{\alpha}(1)(\lambda^0-1)+1} \right).\end{aligned}$$

Inserting this into eq. (C.8), we find for the sampling covariance

$$\sigma_u(s)^2 = \bar{\alpha}(1-s)(\lambda^0-1)+1 + \frac{\bar{\alpha}(1)^2(\lambda^0-1)}{\bar{\alpha}(1-s)} \left(\frac{\bar{\alpha}(1-s)(\lambda^0-1)+1}{\bar{\alpha}(1)(\lambda^0-1)+1} \right)^2$$

Again, since $\bar{\alpha}(1)$ vanishes exponentially with ζ , and $\bar{\alpha}(0) = 1 + \mathcal{O}(h)$, we find that for a long noising trajectory of many steps, $\Sigma_u(1) = \Sigma_0 + \mathcal{O}(h)$ and $\mu_u(1) = \mu_0 + \mathcal{O}(h)$, meaning that the sampling mean and covariance reproduce the empirical mean and covariance of the training set to good approximation.

In the case of finite regularization $\gamma_t = c\sqrt{\bar{\alpha}_t}$, we must replace λ^0 with $\lambda^0 + c$ in all formulae. This shows that both regularization $\bar{\alpha}(0) \neq 1$ bias the sampler towards a covariance matrix with an additional, spherical term.

D Replica theory for linear denoisers at finite N

In this appendix, we derive summary statistics for linear denoisers optimized using the empirical covariance matrix Σ_0 for different sample sizes N . We will assume that the training data originates from a centered Gaussian $\rho \sim \mathcal{N}(0, \Sigma)$, where we define the "true" covariance matrix Σ to be

$$\Sigma = R\Lambda R^T, \quad \Lambda = \begin{pmatrix} \lambda_1 & \dots & 0 \\ \vdots & \ddots & \vdots \\ 0 & \dots & \lambda_d \end{pmatrix}\tag{D.1}$$

with R a fixed rotation matrix, therefore $|R| = 1$, $R^T R = \text{Id}$. We parametrize the empirical covariance matrix $\text{Id} + \hat{\alpha}_t \Sigma_0$ in the following way

$$\Sigma_0 = \frac{1}{N} \sum_{\beta=1}^N \Sigma^{\frac{1}{2}} x^\beta \left(\Sigma^{\frac{1}{2}} x^\beta \right)^T, \quad x^\beta \sim \mathcal{N}(0, \text{Id}) \forall \beta = 1, \dots, N$$

We are now interested in statistics of the inverse of the related random matrix $\text{Id} + \hat{\alpha} \Sigma_0$. We define the following quantities

$$\begin{aligned} f_g(J) &= \frac{1}{d} \int \prod_{\beta} d\rho(x^\beta) \ln Z(J, \Sigma_0) \\ Z(J, \Sigma_0) &:= |\text{Id} + \hat{\alpha} \Sigma_0 + R J g(\Lambda) R^T|^{-\frac{1}{2}} \\ &= \int \frac{d\eta}{\sqrt{2\pi}^d} \exp \left(-\frac{1}{2} \eta^T \left[\text{Id} + \frac{\hat{\alpha}}{N} \sum_{\beta=1}^N \Sigma^{\frac{1}{2}} x^\beta \left(\Sigma^{\frac{1}{2}} x^\beta \right)^T + R J g(\Lambda) R^T \right] \eta \right) \end{aligned} \quad (\text{D.2})$$

The function f then plays the role of a generating functional for the moments of the inverse of $\text{Id} + \hat{\alpha}_t \Sigma_0$, e.g.

$$\frac{1}{d} \left\langle (\text{Id} + \hat{\alpha}_t \Sigma_0)^{-1} \right\rangle_{\Sigma_0} = R \left(-2 \frac{d}{dJ} f(J) \Big|_{J=0, g(\Lambda)=\text{Id}} \right) R^T$$

For the relevant quantities computed in this manuscript, it will be sufficient to compute f for diagonal J , $J_{ij} := \delta_{ij} J_i$. This is because all quantities can be written as traces of matrix products, and choosing J thus corresponds to choosing the basis in which we evaluate the trace to be given by R .

The difficulty in computing f then arises from the fact that all the integrals in x^β are coupled in the logarithm. To evaluate the integral, we now use the replica trick, which consists of re-writing the logarithm as

$$\langle \ln Z(J, \Sigma_0) \rangle_{\Sigma_0} = \lim_{n \rightarrow 0} \frac{1}{n} (\langle Z(J, \Sigma_0) \rangle_{\Sigma_0}^n - 1) \quad (\text{D.3})$$

The replica trick then consists of evaluating $\langle Z(J, \Sigma_0) \rangle_{\Sigma_0}^n$ for integer values of n and then taking the limit $n \rightarrow 0$. To compute $\langle Z(J, \Sigma_0) \rangle_{\Sigma_0}^n$, we first write the power as an integral over n independent variables η^α , where α is the replica index,

$$\langle Z(J, \Sigma_0) \rangle_{\Sigma_0}^n = \int \left(\prod_{\alpha=1}^n \frac{d\eta^\alpha}{\sqrt{2\pi}^d} \right) \left\langle \exp \left(\sum_{\alpha=1}^n -\frac{1}{2} (\eta^\alpha)^T (\text{Id} + \hat{\alpha}_t \Sigma_0 + R J R^T f(\Sigma)) \eta^\alpha \right) \right\rangle_{\Sigma_0} \quad (\text{D.4})$$

In the following section, we will simplify this expression via a change of variables to a set of summary statistics.

D.1 Introducing auxiliary variables

We first isolate the terms depending on x^β from the expression.

$$\begin{aligned} \langle Z \rangle_{\Sigma_0}^n &= \int \left(\prod_{\alpha=1}^n \frac{d\eta^\alpha}{\sqrt{2\pi}^d} \right) \exp \left(\sum_{\alpha=1}^n \left[-\frac{1}{2} (\eta^\alpha)^T (\text{Id} + R J f(\Lambda) R^T) \right] \right) \\ &\quad \cdot \int \left(\prod_{\beta=1}^N \frac{dx^\beta}{\sqrt{2\pi}^d} \right) \exp \left(-\frac{1}{2} \sum_{\beta} (x^\beta)^T \left(\frac{\hat{\alpha}}{N} \sum_{\alpha} \Sigma^{\frac{1}{2}} \eta^\alpha \left(\Sigma^{\frac{1}{2}} \eta^\alpha \right)^T + \text{Id} \right) x^\beta \right) \end{aligned} \quad (\text{D.5})$$

To simplify the expression a bit, we now change variables to $\mu^\alpha = \Sigma^{\frac{1}{2}} \eta^\alpha$, we then find that we can isolate one factor in which Σ appears, but not the samples x^β , and vice versa. Additionally, note that for

given μ^α , the second line is just the N -th power of the first line. Both factors are coupled together by the fact that μ^α appear in both factors. We thus simplify to

$$\langle Z \rangle_{\Sigma_0}^n = \int \left(\prod_{\alpha=1}^n \frac{d\mu^\alpha}{\sqrt{2\pi}^d} \right) \exp \left(-\frac{1}{2} \sum_{\alpha=1}^n (R^T \mu^\alpha)^T \Lambda^{-\frac{1}{2}} (\text{Id} + Jg(\Lambda)) \Lambda^{-\frac{1}{2}} (R^T \mu^\alpha) - \frac{n}{2} \ln |\Lambda| \right) \cdot \left[\underbrace{\int \frac{dx}{\sqrt{2\pi}^d} \exp \left(-\frac{1}{2} x^T \left(\frac{\hat{\alpha}}{N} \sum_{\alpha} \mu^\alpha (\mu^\alpha)^T + \text{Id} \right) x \right)}_{=:G} \right]^N$$

Another rotation of both x^β and μ^α by R^T then eliminates R from the expression, leaving all other terms unchanged. We now simplify the latter integral, G . Our goal is to have all directions i of μ^α decouple. To this end, we define our first auxiliary variable

$$R_\alpha = \frac{1}{\sqrt{d}} x^T \mu^\alpha \quad (\text{D.6})$$

and enforce this definition with a Dirac delta in the integral, using that $\delta(r-m) = \frac{1}{2\pi} \int d\tilde{r} \exp(i\tilde{r}[r-m])$. This yields

$$\begin{aligned} G &= \int \frac{dx}{\sqrt{2\pi}^d} \prod_{\alpha} \frac{dR_{\alpha} d\tilde{R}_{\alpha}}{2\pi} \exp \left(-\frac{1}{2} \frac{d\hat{\alpha}}{N} \sum_{\alpha} R_{\alpha}^2 - \frac{x^2}{2} + i\tilde{R}_{\alpha} \left(R_{\alpha} - \frac{1}{\sqrt{d}} x^T \mu^{\alpha} \right) \right) \\ &= \int \prod_{\alpha} dR_{\alpha} \frac{d\tilde{R}_{\alpha}}{2\pi} \exp \left(-\frac{1}{2} \frac{d\hat{\alpha}}{N} \sum_{\alpha} R_{\alpha}^2 + i\tilde{R}_{\alpha} R_{\alpha} \right) \int \frac{dx}{\sqrt{2\pi}^d} \exp \left(-\frac{x^2}{2} - i \frac{1}{\sqrt{d}} \tilde{R}_{\alpha} x^T \mu^{\alpha} \right) \end{aligned}$$

We see that the integral over x is a Gaussian integral which can be solved exactly, yielding

$$G = \int \prod_{\alpha} dR_{\alpha} \frac{d\tilde{R}_{\alpha}}{2\pi} \exp \left(\sum_{\alpha} \left(-\frac{1}{2} \frac{d\hat{\alpha}}{N} R_{\alpha}^2 + i\tilde{R}_{\alpha} R_{\alpha} \right) - \sum_{\alpha_1, \alpha_2} \frac{\tilde{R}_{\alpha_1} \tilde{R}_{\alpha_2}}{2d} (\mu^{\alpha_1})^T \mu^{\alpha_2} \right)$$

Importantly, this quantity depends only on the replica overlaps $(\mu^{\alpha_1})^T \mu^{\alpha_2}$, which brings us to our second auxiliary variable:

$$Q_{\alpha_1, \alpha_2} := \frac{1}{d} (\mu^{\alpha_1})^T \mu^{\alpha_2} \quad (\text{D.7})$$

Using the Hubbard-Strantonivic transform backwards to also eliminate the integrals over all R_{α} , we find

$$G = \int \sqrt{\frac{N}{d\hat{\alpha}}} \int \prod_{\alpha} \frac{d\tilde{R}_{\alpha}}{\sqrt{2\pi}} \exp \left(-\frac{1}{2} \tilde{R}^T \left(\frac{Q}{d} + \text{Id} \frac{N}{d\hat{\alpha}} \right) R \right) = \sqrt{\frac{N}{d\hat{\alpha}}} \left| Q + \text{Id} \frac{N}{d\hat{\alpha}} \right|^{-\frac{1}{2}}$$

Inserting the result for G into the expression as well as enforcing the definition of Q with another Dirac delta, we find

$$\begin{aligned} \langle Z \rangle_{\Sigma_0}^n &= \prod_i d\rho_i(\lambda_i) \left(\prod_{\alpha_1=1}^n d\mu^{\alpha_1} \prod_{\alpha_2=1}^{\alpha_1} dQ_{\alpha_1, \alpha_2} \frac{d\tilde{Q}_{\alpha_1, \alpha_2}}{2\pi} \right) \exp \left(S \left(\lambda, \{\mu_{\alpha}\}_{\alpha}, Q, \tilde{Q} \right) \right) \\ S \left(\lambda, \{\mu_{\alpha}\}_{\alpha}, P, \tilde{P} \right) &= -\frac{1}{2} \sum_i \left[\lambda_i^{-1} (1 + J_i g(\lambda_i)) \sum_{\alpha} (\mu_i^{\alpha})^2 \right] \\ &\quad + i \sum_{\alpha_1 \leq \alpha_2} \tilde{Q}_{\alpha_1, \alpha_2} \left(Q_{\alpha_1, \alpha_2} - \frac{1}{d} (\mu^{\alpha_1})^T \mu^{\alpha_2} \right) \\ &\quad + N \ln G(Q) - \frac{n}{2} \ln |\lambda_i| \end{aligned}$$

Here we have also explicitly used the fact that we chose J to be diagonal in the eigenspace of Σ . We now also solve the integral over μ^α by exploiting that all spatial directions in the expression are decoupled. The μ^α dependent part of the integral is then given by

$$\begin{aligned} S_i(\tilde{Q}) &= \ln \int \prod_{\alpha} \frac{d\mu_i^{\alpha}}{\sqrt{2\pi}} \exp \left(-\frac{1}{2\lambda_i} (1 + J_i f(\lambda)) \sum_{\alpha} (\mu_i^{\alpha})^2 - \frac{n}{2} \ln |\lambda_i| - \frac{i}{d} \sum_{\alpha_1 \leq \alpha_2} \tilde{Q}_{\alpha_1, \alpha_2} \mu_i^{\alpha_1} \mu_i^{\alpha_2} \right) \\ &= \ln \sqrt{\lambda_i}^{-n} \left| \lambda_i^{-1} \text{Id} (1 + J_i g(\lambda_i)) + \frac{i}{d} \text{diag} \tilde{Q} + \frac{i}{d} \tilde{Q} \right|^{-\frac{1}{2}} \end{aligned}$$

With this, we find that the only remaining integrals are in Q and \tilde{Q} . Assuming that $N, \tilde{Q} = \mathcal{O}(d)$, we now pull out a factor d

$$\begin{aligned} \bar{Z}^n(j) &= \int \prod_{\alpha_1 \leq \alpha_2}^n \frac{dQ_{\alpha_1, \alpha_2} d\tilde{Q}_{\alpha_1, \alpha_2}}{2\pi} \exp \left(dS(Q, \tilde{Q}) \right) \\ S(Q, \tilde{Q}) &= \left[i \sum_{\alpha_1 \leq \alpha_2} \frac{1}{d} \tilde{Q}_{\alpha_1, \alpha_2} Q_{\alpha_1, \alpha_2} + \frac{1}{d} \sum_i S_i(\tilde{Q}) + \frac{N}{d} \ln G(Q) \right] \end{aligned} \quad (\text{D.8})$$

We will not solve these integrals explicitly. Rather, we will approximate the integral by $\exp \left(dS(Q^*, \tilde{Q}^*) \right)$, where Q^*, \tilde{Q}^* are the maxima of S . This is because due to the common prefactor d , the integral is assumed to concentrate around a single point for $d \rightarrow \infty$, the Saddle Point.

D.2 Saddle point approximation for any n

Before we find Q^*, \tilde{Q}^* , we introduce simplification in the form of a replica symmetric Ansatz

$$Q_{\alpha_1, \alpha_2} = q \delta_{\alpha_1, \alpha_2} + p(1 - \delta_{\alpha_1, \alpha_2}) \quad (\text{D.9})$$

$$\frac{i}{d} \tilde{Q} = \tilde{q} \delta_{\alpha_1, \alpha_2} + \tilde{p}(1 - \delta_{\alpha_1, \alpha_2}). \quad (\text{D.10})$$

Parameterizing Q, \tilde{Q} in this way implicitly assumes all replicas are equivalent. With this simplification, we can explicitly diagonalize $Q = n p e_1 e_1^T + (q - p) \text{Id}$ with $\forall i = 1, \dots, n$, where $e_1^\alpha = \frac{1}{\sqrt{n}} \forall \alpha = 1, \dots, n$. Likewise we find $\frac{i}{d} \text{diag} \tilde{Q} + \frac{i}{d} \tilde{Q} = n \tilde{p} e_1 e_1^T + (2\tilde{q} - \tilde{p}) \text{Id}$. Inserting this into the matrix determinant, we find

$$G = \sqrt{\frac{N}{d\hat{\alpha}}}^n \left(q - p + \frac{N}{d\hat{\alpha}} \right)^{-\frac{n}{2}} \left(1 + \frac{np}{q - p + \frac{N}{d\hat{\alpha}}} \right)^{-\frac{1}{2}}$$

and

$$S_i(\tilde{Q}) = -\frac{n-1}{2} \ln |1 + J_i g(\lambda_i) + \lambda_i (2\tilde{q} - \tilde{p})| - \frac{1}{2} \ln |1 + J_i g(\lambda_i) + \lambda_i (2\tilde{q} + (n-1)\tilde{p})| - n \ln \lambda_i$$

We now find and solve the Saddle Point equations: $\frac{d}{da} S = 0$ for $a \in \{q, p, \tilde{q}, \tilde{p}\}$ for $n \in (0, \infty)$. This

yields the following four conditions:

$$\begin{aligned}\tilde{q} &= \frac{N}{2dn} \left(\frac{(n-1)}{q-p+\frac{N}{d\hat{\alpha}}} + \frac{1}{q+(n-1)p+\frac{N}{d\hat{\alpha}}} \right) \\ \tilde{p} &= \frac{N}{dn} \left(-\frac{1}{q-p+\frac{N}{d\hat{\alpha}}} + \frac{1}{q+(n-1)p+\frac{N}{d\hat{\alpha}}} \right) \\ q &= \frac{1}{dn} \sum_i \left[\frac{(n-1)\lambda_i}{1+J_i g(\lambda_i) + \lambda_i(2\tilde{q}-\tilde{p})} + \frac{\lambda_i}{1+J_i g(\lambda_i) + \lambda_i(2\tilde{q}+(n-1)\tilde{p})} \right] \\ p &= \frac{1}{nd} \sum_i \left[\frac{-\lambda_i}{1+J_i g(\lambda_i) + \lambda_i(2\tilde{q}-\tilde{p})} + \frac{\lambda_i}{1+J_i g(\lambda_i) + \lambda_i(2\tilde{q}+(n-1)\tilde{p})} \right]\end{aligned}$$

To simplify these expressions, we make the following observations. First \tilde{q}, \tilde{p} only depend on $u := q - p$ and $w := q + (n-1)p$. Second q, p only depend on $\tilde{u} = 2\tilde{q} - \tilde{p}$ and $\tilde{w} = 2\tilde{q} + (n-1)\tilde{p}$. It is hence possible to re-parametrize the problem and thereby decouple some of the variables. Concretely, using the first two equations, we find

$$\tilde{u} = \frac{N}{d} \frac{1}{u + \frac{N}{d\hat{\alpha}}} \quad \tilde{w} = \frac{N}{d} \left(\frac{1}{w + \frac{N}{d\hat{\alpha}}} \right)$$

The second two equations yield

$$u = \frac{1}{d} \sum_i \left[\frac{\lambda_i}{1+J_i g(\lambda_i) + \lambda_i \tilde{u}} \right] \quad w = \frac{1}{d} \sum_i \left[\frac{\lambda_i}{1+J_i g(\lambda_i) + \lambda_i \tilde{w}} \right]$$

This defines a self-consistency equation each for u, w . Interestingly, both pairs of self-consistency equations are the same. Assuming that the solution is unique, we find that $u = w, \tilde{u} = \tilde{w}$ and hence $p, \tilde{p} = 0$. With this, we find that q must be found self-consistently from

$$q(J) = \frac{1}{d} \sum_i \left[\frac{\lambda_i}{1+J_i g(\lambda_i) + \lambda_i \left(\frac{N}{d} \frac{1}{q + \frac{N}{d\hat{\alpha}}} \right)} \right] \quad (\text{D.11})$$

and

$$\tilde{q} = \frac{N}{2dn} \frac{1}{q + \frac{N}{d\hat{\alpha}}}$$

D.3 Taking the limit $n \rightarrow 0$

Inserting the Saddle-point values for $q, \tilde{q}, p, \tilde{p}$, we find

$$\begin{aligned}\ln \bar{Z}^n(J) &= dn \left[\frac{N}{2d} \frac{q(J)}{q(J) + \frac{N}{d\hat{\alpha}}} - \frac{1}{2d} \sum_i \left[\ln \left| 1 + J_i g(\lambda_i) + \lambda_i \left(\frac{N}{d} \frac{1}{q(J) + \frac{N}{d\hat{\alpha}}} \right) \right| \right] \right. \\ &\quad \left. + \frac{N}{2d} \ln \frac{N}{d\hat{\alpha}} - \frac{N}{2d} \ln \left(q(J) + \frac{N}{d\hat{\alpha}} \right) \right]\end{aligned}$$

Due to the linear appearance of n in $\ln \bar{Z}^n(J)$, we can finally take the limit $n \rightarrow 0$ in eq. (D.3) and find the expression for f

$$f(J) = \frac{N}{2d} \frac{q(J)}{q(J) + \frac{N}{d\hat{\alpha}}} - \left[\frac{1}{2d} \sum_i \ln \left| 1 + J_i g(\lambda_i) + \lambda_i \left(\frac{N}{d} \frac{1}{q(J) + \frac{N}{d\hat{\alpha}}} \right) \right| \right] - \frac{N}{2d} \ln \left(\frac{d\hat{\alpha}}{N} q(J) + 1 \right).$$

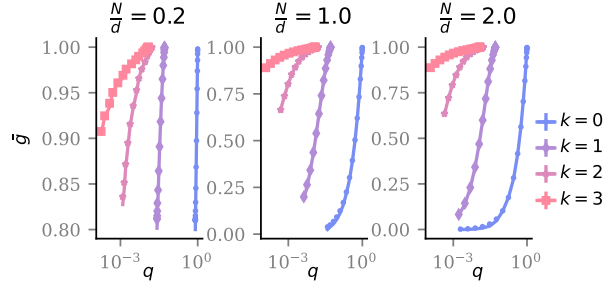


Figure D.1: Relation between \bar{g} and q . Full lines are predictions using eq. (D.16), markers show simulations for different fractions of N/d , and varying values of $\hat{\alpha}$ between 2^{-9} , 2^9 . Colors and marker styles distinguish and different spectra of the true covariance matrix Σ , namely $\lambda_i = i^{-k} \forall i = 1, \dots, d$.

D.4 Consistency checks

To validate our result, we perform a consistency check, using on prior knowledge on the Stieltjes transform g , defined by

$$g(z) = \lim_{d \rightarrow \infty} \frac{1}{d} \text{Tr} \frac{1}{z \text{Id} - \Sigma^{\frac{1}{2}} \mathcal{W} \Sigma^{\frac{1}{2}}}$$

where \mathcal{W} is a Wishart with parameter $q_S = \frac{d}{N}$. It is known that in this case, g fulfills the following self-consistency equation:

$$g(z) = \int d\rho_{\Sigma}(\lambda) \frac{1}{z - \lambda \left(1 - \frac{d}{N} + \frac{d}{N} z g(z)\right)} \quad (\text{D.12})$$

where $\rho_{\Sigma}(\lambda)$ is the spectral density of Σ , $\rho_{\Sigma}(\lambda) = \frac{1}{d} \sum_i \delta(\lambda - \lambda_i)$ in our case. Defining

$$\bar{g} = -\frac{1}{\hat{\alpha}} g\left(-\frac{1}{\hat{\alpha}}\right) = \lim_{d \rightarrow \infty} \frac{1}{d} \text{Tr} \frac{1}{\text{Id} + \hat{\alpha} \Sigma^{\frac{1}{2}} \mathcal{W} \Sigma^{\frac{1}{2}}}$$

this variable then fulfills the self-consistency equation .

$$\bar{g} = \frac{1}{d} \sum_i \frac{1}{1 + \hat{\alpha} \lambda_i \left(1 - \frac{d}{N} + \frac{d}{N} \bar{g}\right)} \quad (\text{D.13})$$

We will now relate the self-consistency relation for g to the self-consistency equation for q . Observe that, from the replica calculation, it follows that

$$\bar{g} = \sum_i \frac{d}{dJ_i} f(J) \Big|_{J=0} = \frac{1}{d} \sum_i \frac{1}{1 + \lambda_i \left(\frac{1}{\hat{\alpha}^{\frac{d}{N} q + 1}}\right)} =: s(q)$$

Using the replica self-consistency relation for q , for $J = 0$, eq. (D.11), we find

$$s(q) := \frac{\hat{\alpha} \left(\frac{d}{N} - 1\right) q + 1}{\hat{\alpha}^{\frac{d}{N} q + 1}}, \quad (\text{D.14})$$

Furthermore, it follows from the definition eq. (D.14), that

$$1 - \frac{d}{N} + \frac{d}{N} s(q) = \frac{1}{\hat{\alpha}^{\frac{d}{N} q + 1}}$$

which, inserted into the definition of s , yields a self-consistency equation for $s(q)$,

$$s(q) = \frac{1}{d} \sum_i \frac{1}{1 + \hat{\alpha} \lambda_i \left(1 - \frac{d}{N} + \frac{d}{N} s(q)\right)} \quad (\text{D.15})$$

which is identical to the self-consistency equation for \bar{g} , eq. (D.13), meaning that the replica calculation produces a variant of the known self-consistency relation eq. (D.12) for the Stieltjes transform. Furthermore the replica calculation yields a relation between $q = \frac{1}{d} \left\langle \text{Tr} \left(\Sigma \frac{1}{1 + \bar{\alpha} \Sigma_0} \right) \right\rangle_{\Sigma_0}$ and $\bar{g} = \frac{1}{d} \left\langle \text{Tr} \left(\frac{1}{1 + \bar{\alpha} \Sigma_0} \right) \right\rangle_{\Sigma_0}$ which is independent of the spectrum of Σ , namely

$$\bar{g} = s(q) \quad (\text{D.16})$$

We test this relation in fig. D.1, finding excellent agreement with simulations.

D.5 Squared difference on test examples

We compute the generalization measure for fixed t :

$$\langle ||(W_t^* - W_t^{\text{oracle}}) x_t||^2 \rangle_{x_t, \Sigma_0} = \frac{1 - \bar{\alpha}_t}{(1 - \bar{\alpha}_t + \gamma_t)} \left(\frac{\psi_{1,1} + \psi_{1,2}}{(1 - \bar{\alpha}_t + \gamma_t)} - 2\psi_2 + \psi_3 \right)$$

where we defined

$$\psi_{1,1}^t = \left\langle \text{Tr} \left[\frac{1 - \bar{\alpha}_t}{(\text{Id} + \hat{\alpha}_t \Sigma_0)^2} \right] \right\rangle \quad \psi_{1,2}^t = \left\langle \text{Tr} \left[\frac{\bar{\alpha}_t}{(\text{Id} + \hat{\alpha}_t \Sigma_0)^2} \Sigma \right] \right\rangle \quad \psi_2^t = \left\langle \text{Tr} \left[\frac{1}{(\text{Id} + \hat{\alpha}_t \Sigma_0)} \right] \right\rangle \quad (\text{D.17})$$

We first compute ψ_2 , using that

$$\psi_2 = -2 \sum_i \frac{d}{dJ_i} f(J) \Big|_{J=0, g=1}$$

We now find $\frac{\partial f(J)}{\partial q} = 0$, hence $\frac{df}{dJ_i} = \frac{\partial f(J)}{\partial J_i}$, which is equal to

$$\frac{df}{dJ_i} = -\frac{1}{2d} \frac{g(\lambda_i)}{1 + J_i g(\lambda_i) + \lambda_i \left(\frac{N}{d} \frac{1}{q + \frac{N}{d\bar{\alpha}}} \right)}$$

Where q is found, e.g. by solving eq. (D.13).

For $\psi_{1,1}$ and $\psi_{1,2}$, we first note that for precision matrix A , and diagonal J, Λ , we have that

$$\frac{d^2}{dJ_i dJ_j} \ln \int \frac{d\eta}{\sqrt{2\pi}^d} \exp \left(-\frac{1}{2} \eta^T [A + Jg(\Lambda)] \eta \right) \Big|_{J=0} = \frac{f(\Lambda)_{ii} f(\Lambda)_{jj}}{2} (A_{ij}^{-1})^2$$

Where we used Wick's theorem to evaluate the Gaussian moments. For the specific functions of interest eq. (D.17), we find

$$\psi_{1,1} = 2 \sum_{ij} \left(\frac{d^2}{dJ_i dJ_j} f(J) \right) \Big|_{J=0, g(x)=1} \quad \psi_{1,2} = 2 \sum_{ij} \left(\frac{d^2}{dJ_i dJ_j} f(J) \right) \Big|_{J=0, g(x)=\sqrt{x}}$$

the only difference between the two being the function g . Hence, we compute the second derivatives

$$\frac{d^2 f}{dJ_i dJ_j} \Big|_{J=0} = \delta_{ij} \frac{1}{2d} \frac{g^2(\lambda_i)}{\left(1 + \lambda_i \left(\frac{N}{d} \frac{1}{q + \frac{N}{d\bar{\alpha}}} \right) \right)^2} - \frac{N}{2d^2} \frac{g(\lambda_i) \lambda_i}{\left(q + \frac{N}{d\bar{\alpha}} + \frac{N}{d} \lambda_i \right)^2} \frac{dq}{dJ_j} \Big|_{J=0}$$

Using the self-consistency equation, we find

$$\left. \frac{dq}{dJ_i} \right|_{J=0} = - \frac{\left(q + \frac{N}{d\hat{\alpha}}\right)^2}{d \left(1 - \frac{N}{d} R_2(q)\right)} \frac{\lambda_i g(\lambda_i)}{\left(q + \frac{N}{d\hat{\alpha}} + \frac{N}{d} \lambda_i\right)^2}$$

where we defined

$$R_k(q) = \frac{1}{d} \sum_j \frac{\lambda_j^k}{\left(q + \frac{N}{d\hat{\alpha}} + \frac{N}{d} \lambda_j\right)^2}.$$

Putting it all together, for the specific functions of interest, we find

$$\psi_{1,1} = \left(q + \frac{N}{d\hat{\alpha}}\right)^2 \left[R_0 + \frac{N}{d} \frac{R_1(q)^2}{\left(1 - \frac{N}{d} R_2(q)\right)} \right] \quad \psi_{1,2} = \left(q + \frac{N}{d\hat{\alpha}}\right)^2 \left[R_1 + \frac{N}{d} \frac{R_{\frac{3}{2}}(q)^2}{\left(1 - \frac{N}{d} R_2(q)\right)} \right]$$

and

$$\psi_2 = \frac{1}{d} \sum_i \frac{1}{1 + \lambda_i \left(\frac{N}{d} \frac{1}{q + \frac{N}{d\hat{\alpha}}}\right)}.$$

D.6 Residual and test loss at finite N

To compute the residual loss, we employ the following identity:

$$\begin{aligned} \left. \frac{df}{d\hat{\alpha}_t} \right|_{J=0, g=1} &= - \frac{1}{2Nd} \sum_{\beta=1}^N \left\langle \sum_{ij} \left(\Sigma^{\frac{1}{2}} x^\beta \right)_i \left(\frac{1}{1 + \hat{\alpha} \Sigma_0} \right)_{ij} \left(\Sigma^{\frac{1}{2}} x^\beta \right)_j \right\rangle \\ &= - \frac{1}{2d} \left\langle \text{Tr} \Sigma_0 \frac{1}{\text{Id} + \hat{\alpha} \Sigma_0} \right\rangle \end{aligned}$$

Inserting this into the equation for the residual loss, eq. (9), which yields

$$\begin{aligned} R &= \frac{-2}{T} \sum_t \frac{\bar{\alpha}_t}{1 - \bar{\alpha}_t + \gamma_t} \left. \frac{df}{d\hat{\alpha}_t} \right|_{J=0, g=1} + \frac{\gamma_t}{1 - \bar{\alpha}_t + \gamma_t} \psi_2 \\ &= \frac{1}{T} \sum_t \frac{\bar{\alpha}_t}{1 - \bar{\alpha}_t + \gamma_t} \frac{q}{\frac{d\hat{\alpha}_t}{N} q + 1} + \frac{\gamma_t}{1 - \bar{\alpha}_t + \gamma_t} \frac{1}{d} \sum_i \frac{1}{1 + \lambda_i \left(\frac{N}{d} \frac{1}{q + \frac{N}{d\hat{\alpha}_t}}\right)} \end{aligned} \quad (\text{D.18})$$

Second, we find that the test loss simplifies to

$$L_{test} = 1 + \frac{1}{T} \sum_t \frac{1 - \bar{\alpha}_t}{(1 - \bar{\alpha}_t + \gamma_t)} \left(\frac{\psi_{1,1} + \psi_{1,2}}{(1 - \bar{\alpha}_t + \gamma_t)} - 2\psi_2 \right)$$

which contains only functions which we have already computed in appendix D.5.

D.7 Kullback-Leibler divergence

We compare $\rho = \mathcal{N}(\mu, \Sigma)$ to $\rho_N = \mathcal{N}(\mu_0, \Sigma_0 + \gamma \text{Id})$. The DKL between two Gaussians is given by eq. (11).

We now average this expression over draws of the data set term by term. First, note that

$$\text{Tr} \Sigma^{-1} (\langle \Sigma_0 \rangle + \gamma \text{Id}) - d = \gamma \text{Tr} \Sigma^{-1} \quad (\text{D.19})$$

Second, we compute

$$\begin{aligned}
\langle (\mu - \mu_0)^T \Sigma^{-1} (\mu - \mu_0) \rangle &= \frac{1}{N^2} \sum_{i,j,k,l=1}^d \sum_{\beta_1, \beta_2=1}^N \langle x_i^{\beta_1} x_j^{\beta_2} \rangle \left(\Sigma^{\frac{1}{2}} + \sqrt{c} \text{Id} \right)_{ki} \Sigma_{kl}^{-1} \left(\Sigma^{\frac{1}{2}} + \sqrt{c} \text{Id} \right)_{lj} \\
&= \frac{1}{N^2} \sum_{i,j=1}^d \sum_{\beta_1, \beta_2=1}^N \delta_{\beta_1 \beta_2} \delta_{ij} \left(1 + 2\sqrt{c} \Sigma_i^{-\frac{1}{2}} j + c \Sigma_i^{-1} j \right) \\
&= \frac{d + 2\sqrt{c} \text{Tr} \Sigma^{-\frac{1}{2}} + c \text{Tr} \Sigma^{-1}}{N}
\end{aligned}$$

with $x^\beta \sim \mathcal{N}(0, \text{Id})$. Finally, we have that when $\gamma = \frac{1}{\hat{\alpha}}$

$$-\frac{1}{2} \langle \ln |\Sigma_0 + \gamma \text{Id}| \rangle = d f(J=0) - \frac{d}{2} \ln \gamma = d f(J=0) + \frac{d}{2} \ln \hat{\alpha} \quad (\text{D.20})$$

we have that

$$df(0) + \frac{d}{2} \ln \hat{\alpha} = \frac{N}{2d} \frac{q}{q + \frac{N}{d\hat{\alpha}}} - \left[\frac{1}{2d} \sum_i \ln \left| \frac{1}{\hat{\alpha}} + \lambda_i \left(\frac{N}{d} \frac{1}{q\hat{\alpha} + \frac{N}{d}} \right) \right| \right] - \frac{N}{2d} \ln \left(\frac{d\hat{\alpha}}{N} q + 1 \right)$$

such that all in all, the DKL simplifies to eq. (15).

D.8 q at $N \gg d$

We now seek an approximation for q in the regime $N \gg d$. To do so, we first examine $\bar{g} = \frac{1}{d} \left\langle \text{Tr} \left(\frac{1}{1 + \hat{\alpha} \Sigma_0} \right) \right\rangle_{\Sigma_0}$, which we found to relate to q via the relation D.16. We now additionally assume that $\hat{\alpha}$ is much larger than $(\lambda_{\min}^0)^{-1}$, where λ_{\min}^0 is the smallest eigenvalue in Σ_0 . This assumption is only valid for at least $N \geq d$ as otherwise Σ_0 has zero eigenvalues. Then it follows that \bar{g} is of order $\hat{\alpha}^{-1}$. We now invert the relation between q and \bar{g} , finding that

$$q = \frac{1}{\hat{\alpha} \frac{d}{N}} \left(\frac{1}{1 - \frac{d}{N} + \frac{d}{N} \bar{g}} - 1 \right) \approx \frac{1}{\hat{\alpha} \frac{d}{N}} \left(\frac{1}{1 - \frac{d}{N}} - 1 \right) \quad (\text{D.21})$$

which is independent of Σ . Inserting this into eq. (15), we find

$$\frac{\text{DKL}(\rho_N | \rho)}{d} = \frac{1 + \frac{N}{d} \ln \left(1 - \frac{d}{N} \right) + \ln \left(1 - \frac{d}{N} \right) + \frac{N}{d^2}}{2} + \mathcal{O} \left(\sqrt{\hat{\alpha}^{-1}} \right), \quad (\text{D.22})$$

which, for $N \gg d$, scales as $\frac{d}{4N}$.